Control of 7-phase permanent magnet synchronous motor drive post three failures

Kamel Saleh[1], Mark Sumner[2]
[1]Department of Electrical Engineering, Faculty of Engineering, An-Najah National University, Nablus, Palestine
[2]Department of Electrical and Electronic Engineering, College of Engineering, Nottingham University, Nottingham, United Kingdom

Article Info

ABSTRACT

The article is introducing a new control technique for the 7-phase permanent magnet synchronous motor (PMSM) drive to enhance its robustness against the failure of phases 'a' and 'c' in addition to the failure of the encoder occurring simultaneously. The article is firstly developing a new multi-dimension space vector pulse width modulation (SVPWM) technique as a part of the fault-tolerant control technique (FTC) to control the magnitudes and angles of the motor's current after the failures of phases 'a' and 'c'. Moreover, the paper is developing another FTC to obtain a sensorless operation of the 7-phase motor after the failure in the encoder while the phase 'a' and 'c' are faulted based on the tracking of the saturation saliency. Simulation results prove that the ripple in the speed post the three failures was maintained to be less than 10 rpm compared to 2 rpm when the 7-phase drive is running without faults. In addition to that, the results demonstrated that the motor responded to instant changes in speeds and loads with a dynamic response very close to that obtained when the 7-phase motor ran under healthy operating conditions.

Corresponding Author:

Kamel Saleh
Department of Electrical Engineering, Faculty of Engineering, An-Najah National University
Nablus, West-Bank, Palestine
Email: kamel.saleh@najah.edu

1. INTRODUCTION

Multi-phase machines have a remarkable advantage in many industrial applications. For example, it is used in applications that demand high power and torque to produce high output power without the need for any increase in the voltage or current such as electric marines. Also, it is used in an application that demand low torque and speed ripples such as electric vehicles. Moreover, it is used in an application that demands a high degree of reliability as it inherently faults tolerant such as electric aircraft [1]–[3].

In the last decades, many efforts have been made in three directions for the multi-phase machines: the first one was devoted to researching the design of the multiphase drive [4]–[8] in terms of the fault-tolerant property. The second direction was devoted to re-searching the modeling of these drives [9], [10]. And the last direction was devoted to re-searching the control techniques of the multi-phase drive [11]–[13].

Among the above-mentioned research areas of multiphase motor drives, the fault-tolerant property has received the most research interest. Hence, many fault-tolerant control techniques (FTC) techniques have been proposed to maintain the operation of the multi-phase machine post the faults. These FTC techniques are classified into active or passive based using a robust fixed control structure or a reconfigured control structure [14]–[17]. Although, the active FTC is difficult to be implement, it can significantly enhance the robustness of the multi-phase drive system.

Whether it is active or passive, most of the FTC techniques are based on obtaining a new distribution of the remaining healthy currents post the faults to maintain magneto motive force (MMF) purely sinusoidal and without harmonics. This distribution of the currents depends on the drive arrangement and the connection of the windings. Also, it depends on the optimization techniques that needed to be achieved post the fault beside maintain the MMF sinusoidal such as maximum torque, minimum losses, and minimum torque ripple [18]–[20]. It is worth saying here that the distribution of the stator current post the faults can be calculated offline using the mathematical model of the multi-phase machine.

However, to achieve the new distribution of the current post-the failures according to the FTC techniques, many kinds of controllers were utilized in the literature. Some of the research used the hysteresis current controller [21]–[23] to implement the FTC technique. Regardless of it is simplicity in implementation, this technique has limited use in the motor drive due to its variable switching frequency. Another control technique that is used in the literature to obtain the new distribution of the currents posts the faults was the vector control technique. Some research used it besides using a modified space vector pulse width modulation (SVPWM) technique [24], [25]. Other research was used besides using a new transformation matrix that considers the new distribution of the currents post the faults [26]–[30]. Besides these techniques, other control techniques have also been used post the faults such as model predictive control [31], direct torque control (DTC) [32], and sliding mode control [33].

The fault in the encoder (speed and position sensor) is another type of fault that has been researched in recent years in multiphase motors. The idea is to obtain the speed and position of the shaft without using the encoder. The techniques that are used to achieve that are model-based techniques, DTC, and voltage and current excitation methods [32]–[36]. Recently, some techniques have been proposed to maintain the operation of the multiphase drive system post the two types of faults which are: the open-circuit fault in one phase of the multi-phase drive in addition to the fault in the encoder [37], [38].

This paper is the first paper that proposed a 7-phase drive capable of running simultaneously after encoder failure, phase 'a' and phase 'c' failures. Firstly, a new multi-dimensional SVPWM has been developed to guarantee proper distribution of the stator currents post the fault in phases 'a' and 'c' according to the minimum current FTC technique. Secondly, the robustness of the drive system is improved by presenting a new technique to determine the shaft speed and position in case of encoder failure while the motor continues to run after phase 'a' and 'c' failures.

2. METHOD
2.1. Fault-tolerant 7-phase permanent magnet synchronous motor (PMSM) drive
2.1.1. 7-phase PMSM dynamic model

The 7-phase PMSM drive system used in this research is shown in Figure 1. A 7-phase inverter is used to supply the motor. The dynamic model of the 7-phase PMSM motor is described in (1)-(2).

$$[v_s] = r_s * [i_s] + l\sigma s * \Delta[i_s] + [e_s] \tag{1}$$

$$j * \Delta\omega = Te - TL + B * \omega \tag{2}$$

where $\Delta = \frac{d}{dt}$, $[v_s] = [v_{sa}, v_{sb}, v_{sc}, v_{sd}, v_{se}, v_{sf}, v_{sg}]^T$ are the stator terminal voltages, $[i_s] = [i_{sa}, i_{sb}, i_{sc}, i_{sd}, i_{se}, i_{sf}, i_{sg}]^T$ are the stator phase currents, $l\sigma s$ is the stator leakage inductance, r_s is the stator resistance, j is the moment of inertia, B damping coefficient, Te is the induced torque, and TL is the load torque. The values of these parameters that are adopted in this paper are given in below. The motor parameters are:
a) $Rated\ voltage = 400\ V$
b) $Rated\ speed = 1500\ rpm$
c) $Rated\ torque = 12\ N.m$
d) $Rated\ power = 2.15\ kW$
e) $kt = 1.2\ N.m/A$
f) $ke = 147\ v/Krpm$
g) $Inertia = 20\ kg/cm2$
h) $R(ph - ph) = 4\ \Omega$
i) $L(ph - ph) = 29.8\ mH$

2.1.2. Healthy operation of 7-phase drive

When the 7-phase motor is operating without faults, the stator currents will be equal in magnitudes and phase shifted by 51.42. This distribution of stator currents is illustrated in Figure 2 and (3) [39]–[41].

Figure 2(a) illustrates the phasor distribution of the stator currents while Figure 2(b) illustrates the sinusoidal distribution of the stator current under healthy operating condition.

$$\begin{bmatrix} i_{sa} \\ i_{sb} \\ i_{sc} \\ i_{sd} \\ i_{se} \\ i_{sf} \\ i_{sg} \end{bmatrix} = \begin{bmatrix} I_m * \cos(\omega t) \\ I_m * \cos(\omega t - 51.42) \\ I_m * \cos(\omega t - 102.85) \\ I_m * \cos(\omega t - 154,28) \\ I_m * \cos(\omega t - 205.71) \\ I_m * \cos(\omega t - 257.14) \\ I_m * \cos(\omega t - 308.57) \end{bmatrix} \tag{3}$$

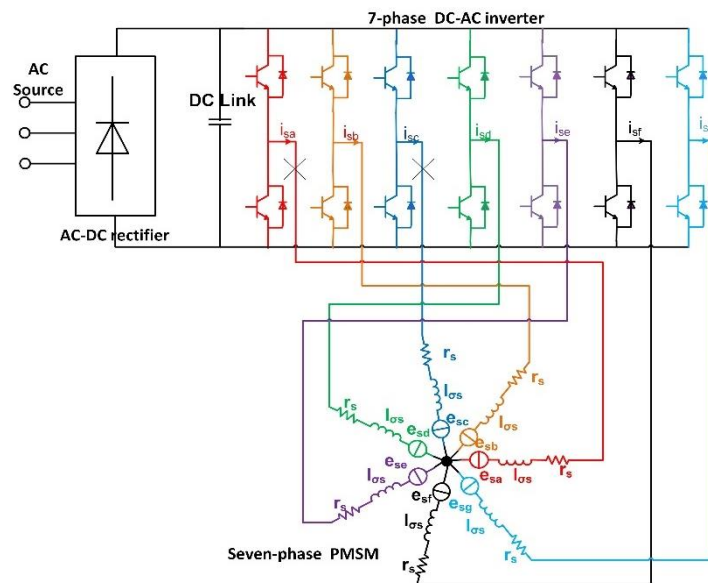where I_m is the peak value of the current in any phase.
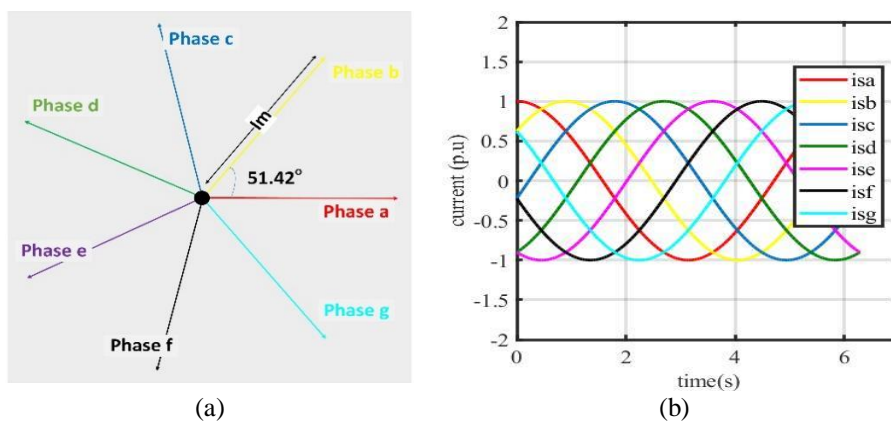

Figure 1. Seven-phase drive topology

| (a) | (b) |

Figure 2. Distribution of the currents in the 7-phase motor running without faults (a) phasor and (b) sinusoidal

2.1.3. Operation of 7-phase drive after the loss of phase 'a'

If a single phase of the 7-phase motor is lost due to a fault, the operation of the 7-phase motor can be maintained by applying a suitable FTC technique. The FTC changes the distribution of the current in the

remaining healthy phases to keep the MMF purely sinusoidal and without harmonics after the fault. In addition, the FTC can also perform other optimizations, such as equal currents, minimum losses, and maximum torque [39]–[42]. If a fault occurs in phase 'a', the remaining healthy currents have to be redistributed as given in (4) and Figure 3 to keep the MMF while minimizing the inverter current [39]–[41]. Figures 3(a) and 3(b) illustrate the phasor and the sinusoidal distribution of the stator currents respectively after the failure in phase 'a'.

$$
\begin{bmatrix} i_{sa} \\ i_{sb} \\ i_{sc} \\ i_{sd} \\ i_{se} \\ i_{sf} \\ i_{sg} \end{bmatrix} = \begin{bmatrix} 0 \\ 1.23 * I_m * \cos(\omega t - 21.4\,°) \\ 1.23 * I_m * \cos(\omega t - 90\,°) \\ 1.23 * I_m * \cos(\omega t - 158.6°) \\ -i_{sa} \\ -i_{sb} \\ -i_{sc} \end{bmatrix} \tag{4}
$$

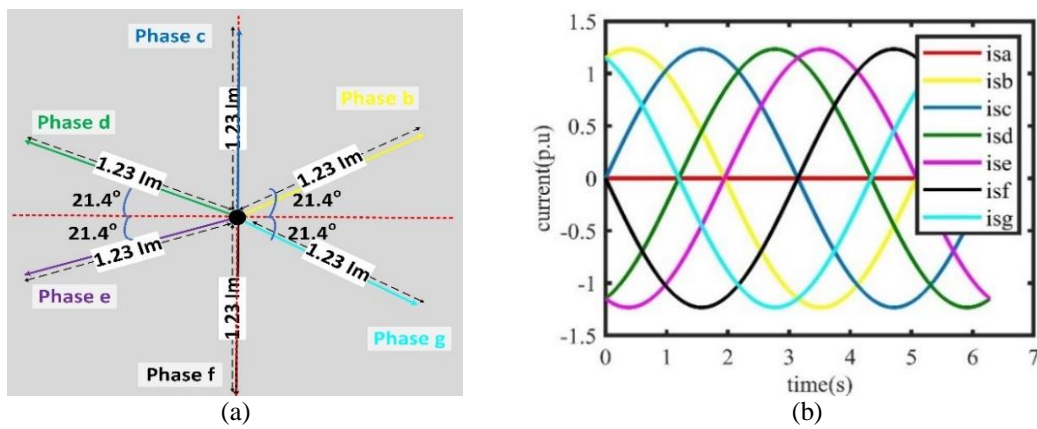(a)   (b)

Figure 3. Distribution of the remaining health current of the 7-phase motor post the loss of phase 'a' to achieve minimum inverter current optimization (a) phasor and (b) sinusoidal

2.1.4. Operation of 7-Phase drive after losing phases 'a' and 'c'

If phases 'a' and 'c' were exposed to a fault, the remaining healthy current has to be redistributed as given in (5) as shown in Figure 4. This distribution will keep the MMF while achieving the minimum the inverter current optimization [39]–[41]. Figures 4(a) and 4(b) illustrates the phasor and sinusoidal distribution of the stator currents respectively after the failure in phases 'a' and 'c'.

$$
\begin{bmatrix} i_{sa} \\ i_{sb} \\ i_{sc} \\ i_{sd} \\ i_{se} \\ i_{sf} \\ i_{sg} \end{bmatrix} = \begin{bmatrix} 0 \\ 1.497\, I_m * \cos(\omega t - 51.4\,°) \\ 0 \\ 1.497\, I_m * \cos(\omega t - 122.6°) \\ 1.497\, I_m * \cos(\omega t - 196.8\,°) \\ 1.497\, I_m * \cos(\omega t - 266.1\,°) \\ 1.497\, I_m * \cos(\omega t - 340.3\,°) \end{bmatrix} \tag{5}
$$

2.2. FTC technique of the 7-phase motor drive after the failures in phases 'a' and 'c'
2.2.1. SVPWM of the 7-phase drive under healthy condition

It is common knowledge that every 3rd or 5th harmonic generated at the output of the 7-phase inverter generates enormous stator currents in the 7-phase motor. This is because these currents are limited only by the stator impedance. Therefore, to generate a pure sinusoidal output of the 7-phase inverter (free from the 3rd and 5th harmonics), multi-dimensional SVPWM is used as shown in Figure 5 [42], [43]. In this modulation technique, the six adjacent vectors of the reference voltage (V_ref) are utilized to synthesize the V_ref in each sector, as shown in Figure 5(a). The adjacent vectors are calculated according to (6):

$$
Vs = \frac{2}{7} VDC \left(S_a + S_b e^{j51.4°} + S_c e^{j102.8°} + S_d e^{j154.2°} + S_e e^{j205.6°} + S_f e^{j257°} + S_g e^{j308.4°} \right) \tag{6}
$$

where $S_a, S_b, S_C, S_D, S_E, S_F$ and S_G are the control signals of the upper switches in each leg of the 7-phase inverter. The pulse width modulation (PWM) waveform for synthesizing the V-ref is depicted in Figure 5(b). The technique to apply the near six vectors-SVPWM (NSV-SVPWM) is illustrated in [42], [43].
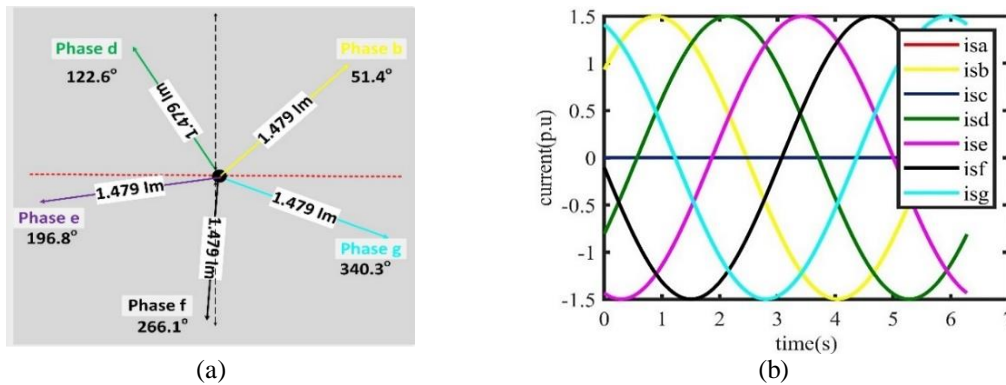

(a)   (b)

Figure 4. Distribution of the current in the 7-phase motor post after the loss of phases 'a' and 'c' to achieve minimum inverter current optimization (a) phasor and (b) sinusoidal
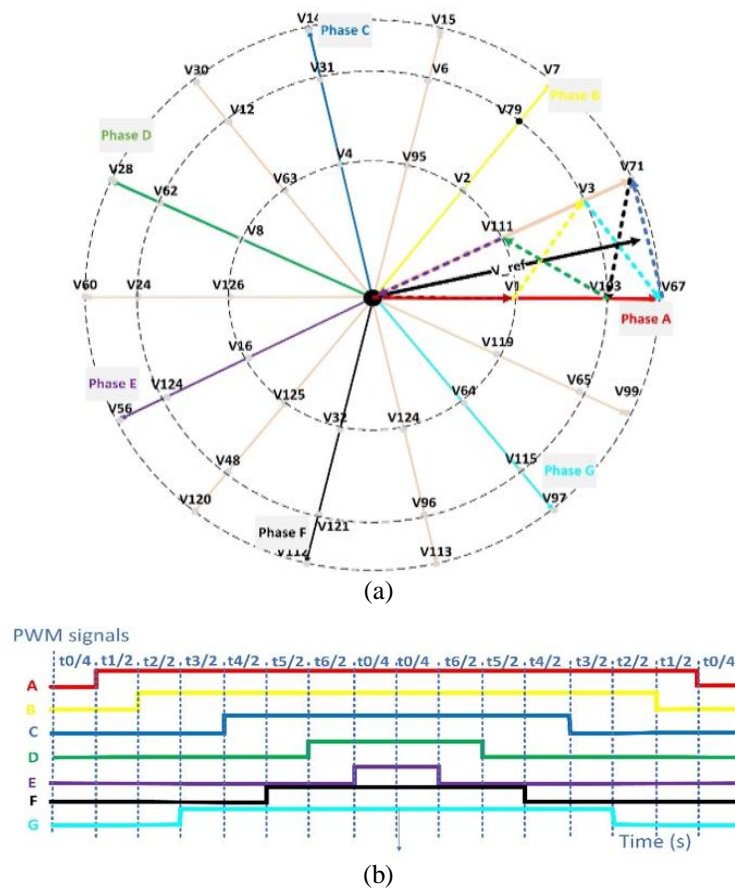

(a)

(b)

Figure 5. 7-phase SVPWM under healthy operating conditions (a) space vector diagram and (b) PWM waveform

2.2.2. SVPWM of the 7-phase drive after losing phase 'a'

When a fault occurs in phase 'a' of the 7-phase drive is lost due to fault, a new SVPWM is proposed in [42] to guarantee a new distribution of the remaining currents to minimize the inverter current as shown in

Figure 6. In this SVPWM technique, the five adjacent vectors were utilized to generate the *V_ref* in each sector as depicted in Figure 6(a). The space vectors are obtained using (7). The PWM waveform for synthesizing the *V_ref* is depicted in Figure 6(b). The procedures to implement the new SVPWM are illustrated in [41].

$$Vs = \frac{2}{7} VDC \left(S_b e^{j21.4°} + S_c e^{j90°} + S_d e^{j158.6°} + S_e e^{j201.4°} + S_f e^{j270°} + S_g e^{j338.6°}\right) \tag{7}$$
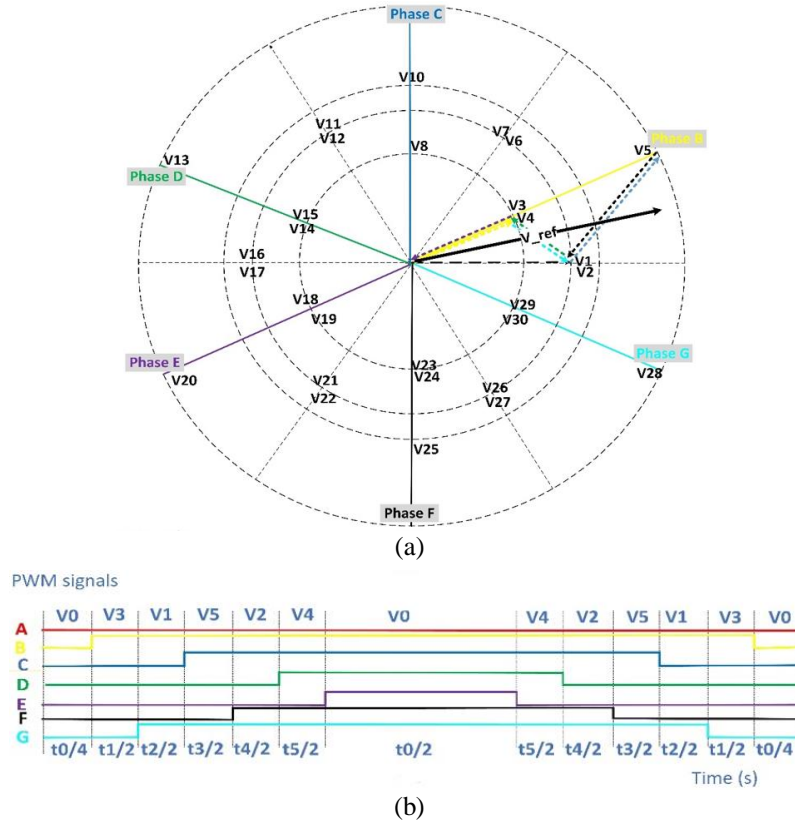

(a)

(b)

Figure 6. 7-phase SVPWM post failure in phase 'a' (a) space vector diagram and (b) PWM waveform

2.2.3. SVPWM of the 7-phase drive after the failures in phases 'a' and 'c'

This paper is presenting a new multidimensional SVPWM technique which is used after the loss of phases 'a' and 'c' to guarantee a new distribution of the currents to achieve the FTC techniques given in (5). The new SVPWM technique which is illustrated in Figure 7 is based on the following assumptions. Firstly, it considers the new distribution of the currents after the failure of phases 'a' and 'c' in the 7-phase drive. In addition, it suppresses any 3rd harmonic at the output of the inverter. This is done by mapping the fundamental component of *V_ref* into the orthogonal stationary frame α1-β1 as shown in Figure 7(a) and mapping the third component of *V_ref* into the orthogonal stationary frame α3-β3 as shown in Figure 7(b). The vectors in α1-β1 and α3-β3 are obtained with (8)-(9). The SVPWWM waveform of this technique is shown in Figure 7(c).

$$Vs1 = \frac{2}{7} VDC \left(S_b e^{j51.4°} + S_d e^{j122.6°} + S_e e^{j2196.8°} + S_f e^{j266.1°} + S_g e^{j340.3°}\right) \tag{8}$$

$$Vs3 = \frac{2}{7} VDC \left(S_b e^{j3*51.4°} + S_d e^{j3*122.6°} + S_e e^{j3*2196.8°} + S_f e^{j3*266.1°} + S_g e^{j3*340.3°}\right) \tag{9}$$

The flowchart depicted in Figure 8 illustrates the procedures for implementing the new SVPWM after the loss of phases 'a' and 'c' in the 7-phase drive. The function of the individual parts is explained as follow: Firstly, according to the location of *V_ref*, the sector is determined as shown in Table 1. Secondly, the dwell time of application of the five vectors adjacent to *V_ref* is calculated according to (10).
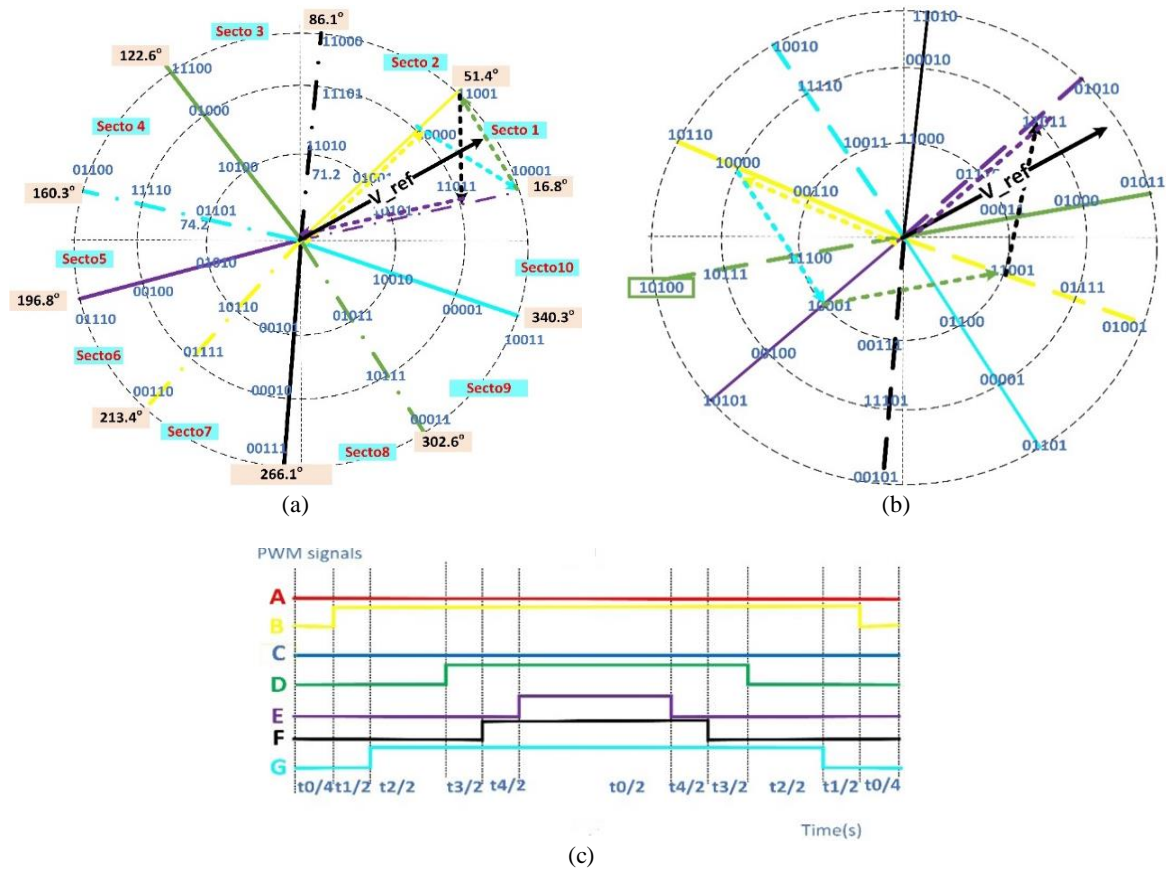
(a)

(b)

(c)

Figure 7. 7-phase SVPWM post failure in phase 'a' and 'c'. (a) space vector diagram in α1-β1 frame, (b) space vector diagram in α3-β3, and (c) PWM waveform
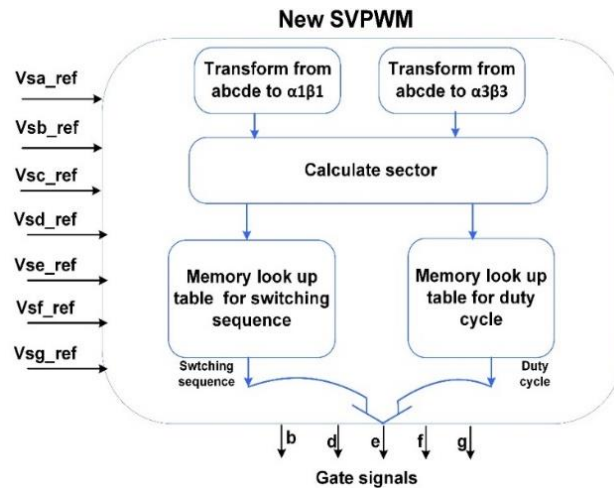

Figure 8. The flowchart illustrates the implementation of the new SVPWM after the loss of phases 'a' and 'c'

Table 1. Selecting the sector

V_ref angle (θ)	Sector no	V_ref angle (θ)	Sector no
$16.8° \leq \theta < 51.4°$	1	$196.8° \leq \theta < 213.4°$	6
$51.4° \leq \theta < 86.1°$	2	$213.4° \leq \theta < 266.1°$	7
$86.1° \leq \theta < 122.6°$	3	$266.1° \leq \theta < 302.6°$	8
$122.6° \leq \theta < 160.3°$	4	$302.6° \leq \theta < 340.3°$	9
$160.3° \leq \theta < 196.8°$	5	$340.3° \leq \theta < 16.8°$	10

$$\begin{bmatrix} V\alpha_1 \\ V\beta_1 \\ V\alpha_3 \\ V\beta_3 \end{bmatrix} * \frac{T_s}{VDC} = \begin{bmatrix} .28*cos(51.4°) & .47*cos(16.8°) & .47*cos(51.4°) & .28*cos(16.8°) \\ .28*sin(51.4°) & .47*sin(16.8°) & .47*sin(51.4°) & .28*sin(16.8°) \\ .28*cos(160.3°) & .16*cos(231.4°) & .16*cos(340.3°) & .28*cos(51.4°) \\ .28*sin(160.3°) & .16*sin(231.4°) & .16*sin(340.3°) & .28*sin(51.4°) \end{bmatrix} * \begin{bmatrix} t1 \\ t2 \\ t3 \\ t4 \end{bmatrix} \quad (10)$$

where $V\alpha_1, V\beta_1, V\alpha_3$, and $V\beta_3$ are the components of V_ref in the $\alpha1 - \beta1$ and $\alpha3 - \beta3$ frames, T_s is the time for one PWM period. Solving (10) gives (11)-(12).

$$\begin{bmatrix} t1 \\ t2 \\ t3 \\ t4 \end{bmatrix} = \frac{T_s}{VDC} * \begin{bmatrix} -0.4675 & 1.5473 & -2.1329 & 1.7038 \\ 2.16 & -1.7251 & -0.5601 & -1.5609 \\ -0.7983 & 2.6454 & 1.2957 & -1.0351 \\ 1.262 & -1.0072 & 0.922 & 2.5694 \end{bmatrix} * \begin{bmatrix} V\alpha_1 \\ V\beta_1 \\ V\alpha_3 \\ V\beta_3 \end{bmatrix} \quad (11)$$

$$t0 = T_s - t1 - t2 - t3 - t4 \quad (12)$$

The timing in addition to the order of the application of each vector in each sector to generate the V_ref in the new SVPWM is illustrated in Table 2.

Table 2. Timing and switching order in each sector in the new SVPWM

Sector no	dwell Time		Switching order
1	$\begin{bmatrix} t1 \\ t2 \\ t3 \\ t4 \end{bmatrix} =* \frac{T}{VDC} \begin{bmatrix} -0.46 & 1.54 & -2.13 & 1.70 \\ 2.16 & -1.72 & -0.56 & -1.56 \\ -0.79 & 2.64 & 1.29 & -1.03 \\ 1.262 & -1.00 & 0.92 & 2.56 \end{bmatrix} *$	$\begin{bmatrix} V\alpha_1 \\ V\beta_1 \\ V\alpha_3 \\ V\beta_3 \end{bmatrix}$	10000,10001,11001,11011
2	$\begin{bmatrix} t1 \\ t2 \\ t3 \\ t4 \end{bmatrix} =* \frac{T}{VDC} \begin{bmatrix} 1.60 & -0.11 & 2.67 & 0.18 \\ -2.15 & 1.72 & 0.55 & 1.53 \\ 2.75 & -0.18 & 1.62 & -0.11 \\ -1.26 & 1.00 & -0.90 & 2.52 \end{bmatrix} *$	$\begin{bmatrix} V\alpha_1 \\ V\beta_1 \\ V\alpha_3 \\ V\beta_3 \end{bmatrix}$	10000,11000,11001,11101
3	$\begin{bmatrix} t1 \\ t2 \\ t3 \\ t4 \end{bmatrix} =* \frac{T}{VDC} \begin{bmatrix} -1.53 & 0.10 & 2.75 & -0.18 \\ 2.22 & 1.42 & -0.48 & 1.60 \\ -2.63 & 0.18 & -1.67 & 0.11 \\ 1.30 & 0.83 & 0.80 & -2.54 \end{bmatrix} *$	$\begin{bmatrix} V\alpha_1 \\ V\beta_1 \\ V\alpha_3 \\ V\beta_3 \end{bmatrix}$	01000,11000,11100,11101
4	$\begin{bmatrix} t1 \\ t2 \\ t3 \\ t4 \end{bmatrix} =* \frac{T}{VDC} \begin{bmatrix} 0.50 & 1.41 & 2.26 & 1.44 \\ -2.16 & -1.38 & 0.47 & -1.56 \\ 0.86 & 2.41 & -1.37 & -0.87 \\ -1.26 & -0.80 & -0.7753 & 2.56 \end{bmatrix} *$	$\begin{bmatrix} V\alpha_1 \\ V\beta_1 \\ V\alpha_3 \\ V\beta_3 \end{bmatrix}$	01000, 01100, 11100, 11110
5	$\begin{bmatrix} t1 \\ t2 \\ t3 \\ t4 \end{bmatrix} =* \frac{T}{VDC} \begin{bmatrix} -0.50 & -1.45 & -2.30 & -1.46 \\ -0.76 & 2.52 & 1.30 & -1.03 \\ -0.89 & -2.48 & 1.40 & 0.90 \\ -0.44 & 1.47 & -2.13 & 1.70 \end{bmatrix} *$	$\begin{bmatrix} V\alpha_1 \\ V\beta_1 \\ V\alpha_3 \\ V\beta_3 \end{bmatrix}$	00100, 01100, 01110, 11110
6	$\begin{bmatrix} t1 \\ t2 \\ t3 \\ t4 \end{bmatrix} =* \frac{T}{VDC} \begin{bmatrix} -1.26 & 1.00 & -0.92 & -2.57 \\ 0.80 & -2.64 & -1.30 & 1.03 \\ -2.16 & 1.72 & 0.56 & 1.56 \\ 0.46 & -1.54 & 2.13 & -1.70 \end{bmatrix} *$	$\begin{bmatrix} V\alpha_1 \\ V\beta_1 \\ V\alpha_3 \\ V\beta_3 \end{bmatrix}$	00100, 00110, 01110, 01111
7	$\begin{bmatrix} t1 \\ t2 \\ t3 \\ t4 \end{bmatrix} =* \frac{T}{VDC} \begin{bmatrix} 1.26 & -1.00 & 0.90 & 2.52 \\ -2.75 & 0.19 & -1.62 & 0.11 \\ 2.15 & -1.72 & -0.55 & -1.53 \\ -1.60 & 0.11 & 2.67 & -0.18 \end{bmatrix} *$	$\begin{bmatrix} V\alpha_1 \\ V\beta_1 \\ V\alpha_3 \\ V\beta_3 \end{bmatrix}$	00010, 00110, 00111, 01111
8	$\begin{bmatrix} t1 \\ t2 \\ t3 \\ t4 \end{bmatrix} =* \frac{T}{VDC} \begin{bmatrix} -1.30 & -0.83 & -0.80 & 2.64 \\ 2.63 & -0.18 & 1.67 & -0.11 \\ -2.22 & -1.42 & 0.48 & -1.60 \\ 1.54 & -0.10 & -2.67 & 0.19 \end{bmatrix} *$	$\begin{bmatrix} V\alpha_1 \\ V\beta_1 \\ V\alpha_3 \\ V\beta_3 \end{bmatrix}$	00010, 00011, 10011, 10111
9	$\begin{bmatrix} t1 \\ t2 \\ t3 \\ t4 \end{bmatrix} =* \frac{T}{VDC} \begin{bmatrix} 1.26 & 0.80 & 0.77 & -2.57 \\ -0.86 & -2.41 & 1.37 & 0.87 \\ 2.21 & 1.38 & -0.47 & 1.56 \\ -0.50 & -1.40 & -2.26 & 1.44 \end{bmatrix} *$	$\begin{bmatrix} V\alpha_1 \\ V\beta_1 \\ V\alpha_3 \\ V\beta_3 \end{bmatrix}$	00001,00011,10011,10111
10	$\begin{bmatrix} t1 \\ t2 \\ t3 \\ t4 \end{bmatrix} =* \frac{T}{VDC} \begin{bmatrix} 0.44 & -1.47 & 2.13 & -1.70 \\ 0.90 & 2.48 & -1.40 & -0.90 \\ 0.76 & -2.52 & -1.29 & 1.03 \\ 0.52 & 1.44 & 2.3 & 1.47 \end{bmatrix} *$	$\begin{bmatrix} V\alpha_1 \\ V\beta_1 \\ V\alpha_3 \\ V\beta_3 \end{bmatrix}$	00001,10001,10011,11011

2.2.4. Simulation results for sensored control of 7-phase drive after losing phases 'a' and 'c'

The proposed FTC technique suggested in the previous section after the loss of phases 'a' and 'c' was implemented using the SABRE simulator as shown in Figure 9. Under healthy operating conditions, the SVPWM technique presented in [36] was utilized. In case of failure of phase 'a', the SVPWM presented in [41] was utilized. If the failure occurred in phases 'a' and 'c', the new SVPWM proposed in the previous

section was used. It should be mentioned here that the switching frequency was set to 5 kHz in all cases. In addition, the encoder was used to obtain the speed and position of the motor to achieve vector control. The result of the test described above is depicted in Figure 10. The 7-phase motor was running at half load under healthy operating conditions. The encoder results show that the speed of the shaft of the 7-phase motor was 120 rpm. Furthermore, the waveforms of the stator current show that the SVPWM technique succeeded in suppressing the 3rd and 5th harmonics in the stator current and achieving a symmetrical distribution of the stator current with a phase shift of 51.4 as shown in (3).
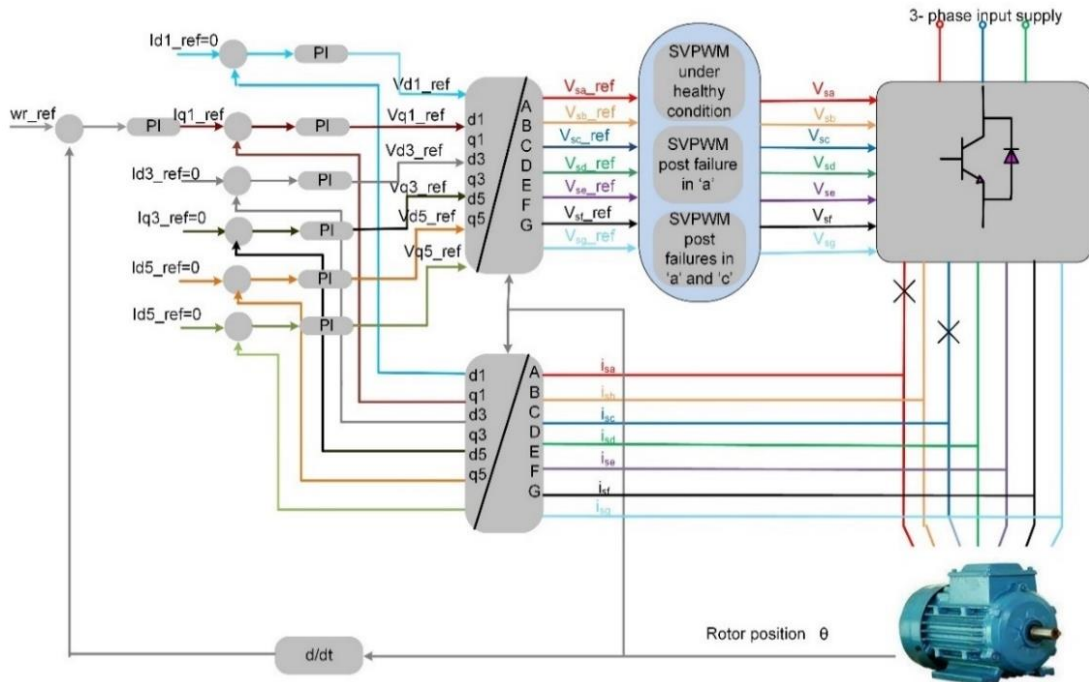

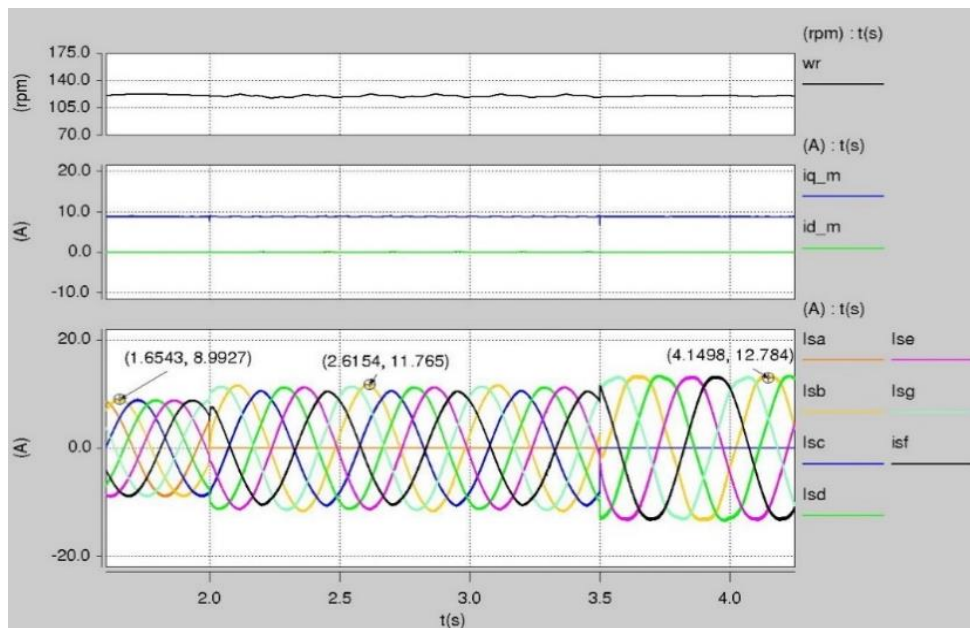Figure 9. 7-sensored control structure of the 7-phase drive post the failures in phases 'a' and 'c'

Figure 10. Simulation results of the FTC technique proposed for the 7-phase drive after the loss of phases 'a' and 'c'

After that when $t = 2\ s$, a fault occurred in phase 'a', and the space vector pulse width modulation (SVPWM) proposed in [41] was utilized simultaneously. The measured speed of the motor obtained using the encoder proves that the 7-phase motor speed was not changed but the ripple in speed was slightly increased. In addition, the other waveforms of the stator current showed that the SVPWM technique succeeded in suppressing the 3rd and 5th harmonics in the stator current and achieving a new distribution of the stator current with a 23% increase in amplitude and a phase shift similar to that given in (4). Finally, at $t = 3.5\ s$, faults occurred in phases 'a' and 'c', and the new SVPWM technique proposed in this paper was applied simultaneously. The results prove that the measured speed of the 7-phase drive obtained using the encoder was not changed and the ripple in the speed was not changed too. From the remaining waveforms of the stator currents, it can be seen that the SVPWM technique suppresses any 3rd harmonic in the stator current and achieves a new distribution of the stator current with a 49.7% increase in amplitude and a phase shift similar to that given in (4).

2.3. FTC technique of the 7-phase motor after the failure in the encoder while phases 'a' and 'c' are faulted

2.3.1. Algorithm to obtain the speed and position of the 7-phase motor after the failure in the encoder

In this section, a new algorithm has been proposed in this paper to determine the shaft speed and position after the encoder failure, while the motor continues to run after the failure of phases 'a' and 'c'. This procedure is help to enhance the stability of the 7-phase PMSM drive significantly. Unfortunately, the algorithms introduced in [36] and [41] to determine the shaft speed and position in the 7-phase motor running under healthy operating conditions and after a failure of phase 'a', respectively, are no longer applicable after the failure of phases 'a' and 'c'. The reason for this is that the derivative of the stator currents in the faulty phases 'a' and 'c' becomes zero after the fault. Moreover, the implementation of the new SVPWM after the failures in phases 'a' and 'c' as part of the FTC technique changes the switching operations of the 7-phase inverter, which affects the algorithms proposed in [36] and [41] to determine the shaft speed and position. Therefore, in this paper, a new algorithm is developed to determine the shaft position and speed of the 7-phase motor after the failure of phases 'a' and 'c'. This algorithm is considering the use of the new SVPWM technique presented in the previous section as a part of the FTC technique in the 7-phase drive after the loss of phases 'a' and 'c'.

Figure 11 illustrates the technique used to track the saliency of the 7-phase drive post the failure in phases 'a' and 'c' using the transient current responses. Figure 11(a) shows how can the neighboring active vectors be used to generate the *V_ref* in sector no 1. Figure 11(b) illustrates the PWM signals in one period related to the application of the neighboring vectors and the sampling instance for measuring the stator current derivatives in one PWM period.

The equivalent circuits of the 7-phase motor after the loss of phases 'a' and 'c' during applying the neighboring vectors according to the new SVPWM are depicted in Figure 12. Figures 12(a) illustrates the equivalent circuit of the 7-phase motor when the zero vector V0 (00000) is applied. Figures 12(b)-12(e) represent the equivalent circuits of the 7-phase motor when the active vectors V1(10000), V2(10001), V3(11001), V4(11011) are applied respectively.

Based on the above circuits, the (13)–(18) can be written:

$$\begin{bmatrix} VDC \\ 0 \end{bmatrix} = r_s * \begin{bmatrix} i_{sb}{}^{V1} \\ i_{sg}{}^{V1} \end{bmatrix} + \begin{bmatrix} l_{\sigma sb} * \Delta\left(i_{sb}{}^{V1}\right) \\ l_{\sigma sg} * \Delta\left(i_{sg}{}^{V1}\right) \end{bmatrix} + \begin{bmatrix} e_{sb}{}^{V1} \\ e_{sg}{}^{V1} \end{bmatrix} \tag{13}$$

$$\begin{bmatrix} VDC \\ 0 \end{bmatrix} = r_s * \begin{bmatrix} i_{sb}{}^{V1} \\ i_{sg}{}^{V1} \end{bmatrix} + \begin{bmatrix} l_{\sigma sb} * \Delta\left(i_{sb}{}^{V1}\right) \\ l_{\sigma sg} * \Delta\left(i_{sg}{}^{V1}\right) \end{bmatrix} + \begin{bmatrix} e_{sb}{}^{V1} \\ e_{sg}{}^{V1} \end{bmatrix} \tag{14}$$

$$\begin{bmatrix} VDC \\ 0 \end{bmatrix} = r_s * \begin{bmatrix} i_{sg}{}^{V2} \\ i_{sd}{}^{V2} \end{bmatrix} + \begin{bmatrix} l_{\sigma sg} * \Delta\left(i_{sg}{}^{V2}\right) \\ l_{\sigma sd} * \Delta\left(i_{sd}{}^{V2}\right) \end{bmatrix} + \begin{bmatrix} e_{sg}{}^{V2} \\ e_{sd}{}^{V2} \end{bmatrix} \tag{15}$$

$$\begin{bmatrix} VDC \\ 0 \end{bmatrix} = r_s * \begin{bmatrix} i_{sd}{}^{V3} \\ i_{sf}{}^{V3} \end{bmatrix} + \begin{bmatrix} l_{\sigma sd} * \Delta\left(i_{sd}{}^{V3}\right) \\ l_{\sigma sf} * \Delta\left(i_{sf}{}^{V3}\right) \end{bmatrix} + \begin{bmatrix} e_{sd}{}^{V3} \\ e_{sf}{}^{V3} \end{bmatrix} \tag{16}$$

$$\begin{bmatrix} VDC \\ 0 \end{bmatrix} = r_s * \begin{bmatrix} i_{sf}{}^{V4} \\ i_{se}{}^{V4} \end{bmatrix} + \begin{bmatrix} l_{\sigma sf} * \Delta\left(i_{sf}{}^{V4}\right) \\ l_{\sigma se} * \Delta\left(i_{se}{}^{V4}\right) \end{bmatrix} + \begin{bmatrix} e_{sf}{}^{V4} \\ e_{se}{}^{V4} \end{bmatrix} \tag{17}$$

$$[VDC] = r_s * [i_{se}{}^{V0}] + [l_{\sigma se} * \Delta(i_{se}{}^{V0})] + [e_{se}{}^{V0}] \tag{18}$$

If the voltage drops on r_s and the back emf are neglected as in [42], can be written as (19).

$$\begin{bmatrix} VDC \\ VDC \\ VDC \\ VDC \\ VDC \\ VDC \end{bmatrix} = \begin{bmatrix} l_{\sigma sb} * \Delta(i_{sb}{}^{V1} - i_{sb}{}^{V0}) \\ l_{\sigma sd} * \Delta(i_{sd}{}^{V3} - i_{sd}{}^{V2}) \\ l_{\sigma se} * \Delta(i_{se}{}^{V1} - i_{se}{}^{V0}) \\ l_{\sigma sf} * \Delta(i_{sf}{}^{V4} - i_{sf}{}^{V3}) \\ l_{\sigma sg} * \Delta(i_{sg}{}^{V0} - i_{sg}{}^{V4}) \end{bmatrix} \tag{19}$$

The position scalars $p_{sb}, p_{sd}, p_{se}, p_{sf}$, and p_{sg} can be written as (20).

$$\begin{bmatrix} p_{sb} \\ p_{sc} \\ p_{sd} \\ p_{se} \\ p_{sf} \\ p_{sg} \end{bmatrix} = \begin{bmatrix} \Delta(i_{sb}{}^{V1} - i_{sb}{}^{V0}) \\ \Delta(i_{sd}{}^{V3} - i_{sd}{}^{V2}) \\ \Delta(i_{se}{}^{V0} - i_{se}{}^{V4}) \\ \Delta(i_{sf}{}^{V4} - i_{sf}{}^{V3}) \\ \Delta(i_{sg}{}^{V2} - i_{sg}{}^{V1}) \end{bmatrix} \tag{20}$$
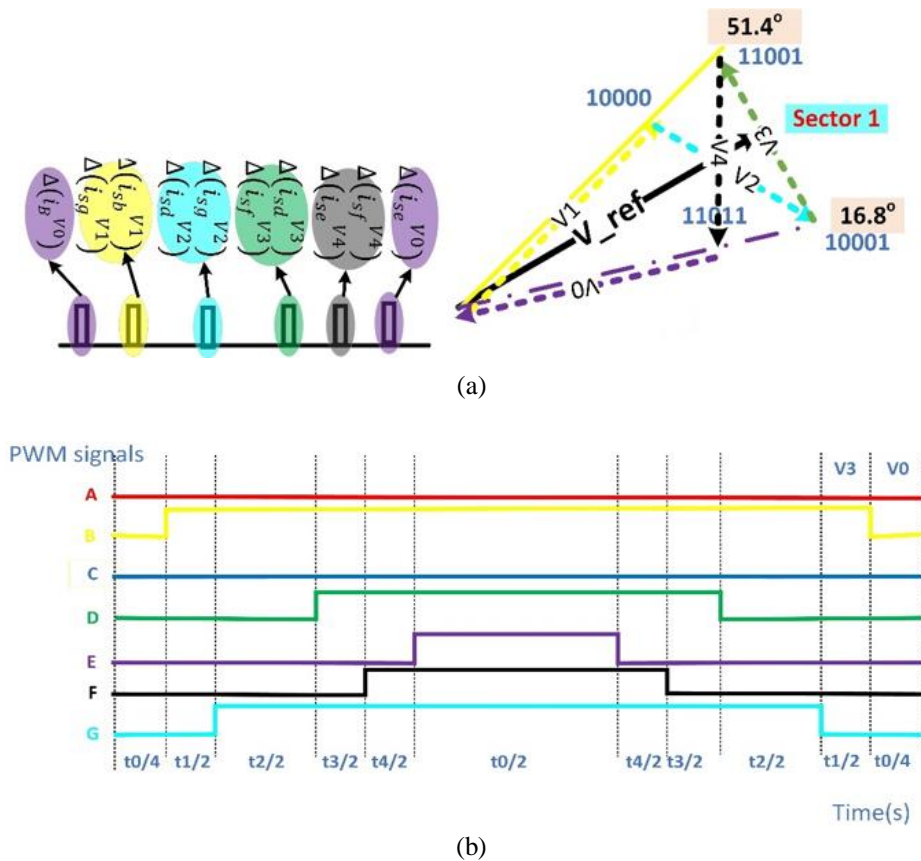

(a)

(b)

Figure 11. SVPWM technique and the associated sampling instant in sector 1 of the 7-phase drive after the loss of phases 'a' and 'c' (a) synthesizing *V_ref* and (b) PWM waveform and sampling instants

The (13)–(20) are applied to the other sectors to obtain the position signals. The position scalars in all sectors are given in Table 3. These position signals can be used then to obtain the position scalars $p\alpha, p\beta$ as shown in (21).

$$\begin{bmatrix} p_\alpha \\ p_\beta \end{bmatrix} = [V] \begin{bmatrix} p_{sb} \\ p_{sc} \\ p_{sd} \\ p_{se} \\ p_{sf} \\ p_{sg} \end{bmatrix} \tag{21}$$

where

$$V = \begin{bmatrix} \cos(102.8°) & \cos(225.2°) & \cos(33.6°) & \cos(172.2°) & \cos(320.6°) \\ \sin(102.8°) & \sin(225.2°) & \sin(33.6°) & \sin(172.2°) & \sin(320.6°) \end{bmatrix} \tag{22}$$

(a)   (b)   (c)
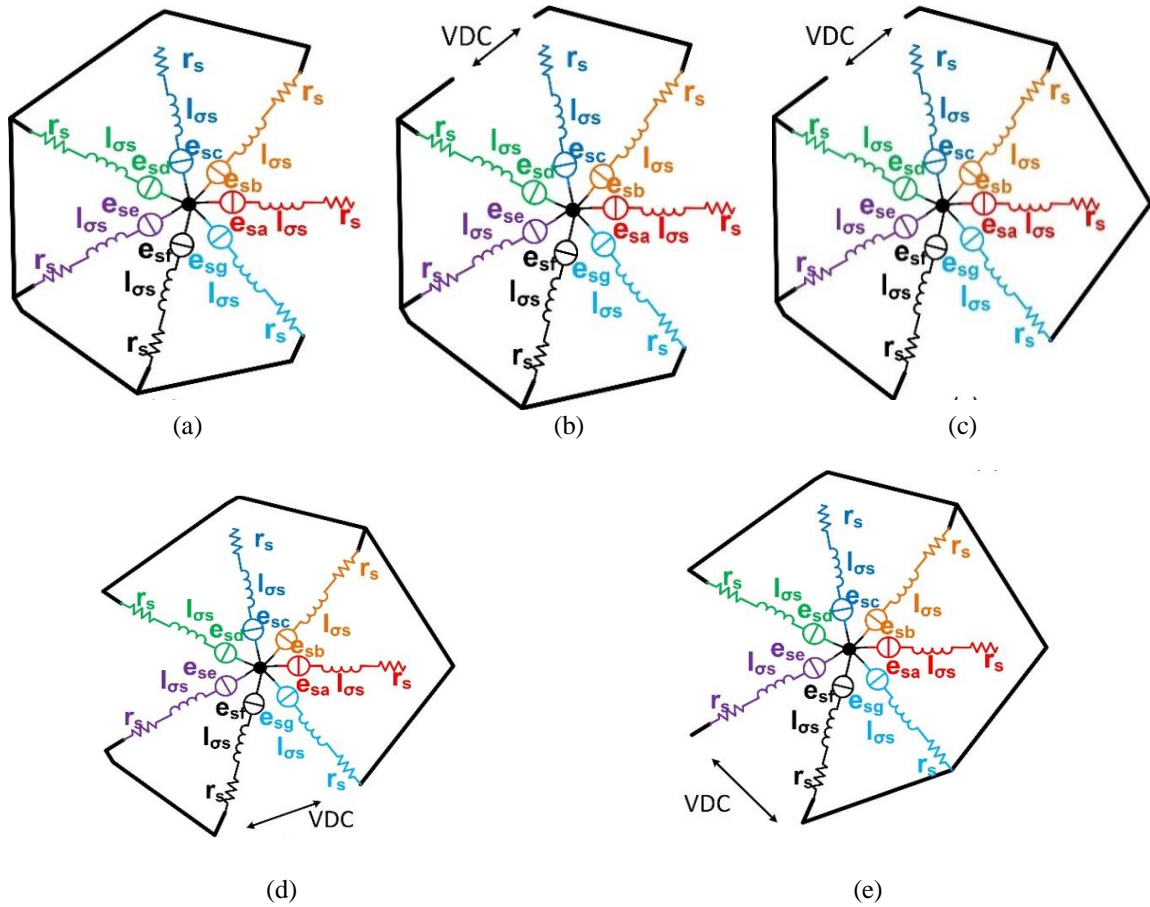
(d)   (e)

Figure 12. Equivalent circuit of the 7-phase PMSM after the loss of phases 'a' and 'c' when active vectors:
(a) V0 was applied, (b) V1 was applied, (c) V2 was applied, (d) V3 was applied, and (e) V4 was applied

Table 3. Formulas to get the position signals in all sectors after the loss of phases 'a' and 'c'

Sector	p_{sb}	p_{sd}	p_{se}	p_{sf}	p_{sg}
1	$\Delta(i_{sb}^{V1} - i_{sb}^{V0})$	$(i_{sd}^{V3} - i_{sd}^{V2})$	$\Delta(i_{se}^{V0} - i_{se}^{V4})$	$\Delta(i_{sf}^{V4} - i_{sf}^{V3})$	$\Delta(i_{sg}^{V2} - i_{sg}^{V1})$
2	$\Delta(i_{sb}^{V1} - i_{sb}^{V0})$	$(i_{sd}^{V2} - i_{sd}^{V1})$	$\Delta(i_{se}^{V4} - i_{se}^{V3})$	$\Delta(i_{sf}^{V0} - i_{sf}^{V4})$	$\Delta(i_{sg}^{V3} - i_{sg}^{V2})$
3	$\Delta(i_{sb}^{V2} - i_{sb}^{V1})$	$(i_{sd}^{V1} - i_{sd}^{V0})$	$\Delta(i_{se}^{V3} - i_{se}^{V2})$	$\Delta(i_{sf}^{V0} - i_{sf}^{V4})$	$\Delta(i_{sg}^{V4} - i_{sg}^{V3})$
4	$\Delta(i_{sb}^{V3} - i_{sb}^{V2})$	$(i_{sd}^{V1} - i_{sd}^{V0})$	$\Delta(i_{se}^{V2} - i_{se}^{V1})$	$\Delta(i_{sf}^{V4} - i_{sf}^{V3})$	$\Delta(i_{sg}^{V0} - i_{sg}^{V4})$
5	$\Delta(i_{sb}^{V4} - i_{sb}^{V3})$	$(i_{sd}^{V2} - i_{sd}^{V1})$	$\Delta(i_{se}^{V1} - i_{se}^{V0})$	$\Delta(i_{sf}^{V3} - i_{sf}^{V2})$	$\Delta(i_{sg}^{V4} - i_{sg}^{V0})$
6	$\Delta(i_{sb}^{V0} - i_{sb}^{V4})$	$(i_{sd}^{V3} - i_{sd}^{V2})$	$\Delta(i_{se}^{V1} - i_{se}^{V0})$	$\Delta(i_{sf}^{V2} - i_{sf}^{V1})$	$\Delta(i_{sg}^{V4} - i_{sg}^{V3})$
7	$\Delta(i_{sb}^{V0} - i_{sb}^{V4})$	$(i_{sd}^{V4} - i_{sd}^{V3})$	$\Delta(i_{se}^{V2} - i_{se}^{V1})$	$\Delta(i_{sf}^{V1} - i_{sf}^{V0})$	$\Delta(i_{sg}^{V3} - i_{sg}^{V2})$
8	$\Delta(i_{sb}^{V4} - i_{sb}^{V3})$	$(i_{sd}^{V0} - i_{sd}^{V4})$	$\Delta(i_{se}^{V3} - i_{se}^{V2})$	$\Delta(i_{sf}^{V1} - i_{sf}^{V0})$	$\Delta(i_{sg}^{V2} - i_{sg}^{V1})$
9	$\Delta(i_{sb}^{V3} - i_{sb}^{V2})$	$(i_{sd}^{V0} - i_{sd}^{V4})$	$\Delta(i_{se}^{V4} - i_{se}^{V3})$	$\Delta(i_{sf}^{V2} - i_{sf}^{V1})$	$\Delta(i_{sg}^{V1} - i_{sg}^{V0})$
10	$\Delta(i_{sb}^{V2} - i_{sb}^{V1})$	$(i_{sd}^{V4} - i_{sd}^{V3})$	$\Delta(i_{se}^{V0} - i_{se}^{V4})$	$\Delta(i_{sf}^{V3} - i_{sf}^{V2})$	$\Delta(i_{sg}^{V1} - i_{sg}^{V0})$

2.3.2. Simulation results for the shaft speed and position signals in the 7-phase motor drive after the loss of phases 'a' and 'c'

The algorithm to get speed and position in the 7-phase drive after the failures in phases 'a' and 'c' was simulated in the SABER simulator see Figure 13. Firstly, the transient current waveforms *(Δ(isa, isb, isc, isd, ise, isf,* and *isg))* of the 7-phase motor were sampled after 10 us of each IGBT switching action to allow the oscillation to decay and reduce noise, hence a minimum pulse width of 10 us was introduced. Secondly, based on the operation, the algorithm for determining the shaft speed and position was selected (i.e., healthy condition [36], phase 'a' fault [41], and phase 'a' and 'c' faults). Finally, the position signals obtained from these algorithms were used by a mechanical observer [44] to filter out the noises and obtain a clean estimated position and velocity signal. Note that if the dwell time for any vector was less than 10 us, it is extended to 10 us to assure the decaying of any oscillation in the current derivatives.
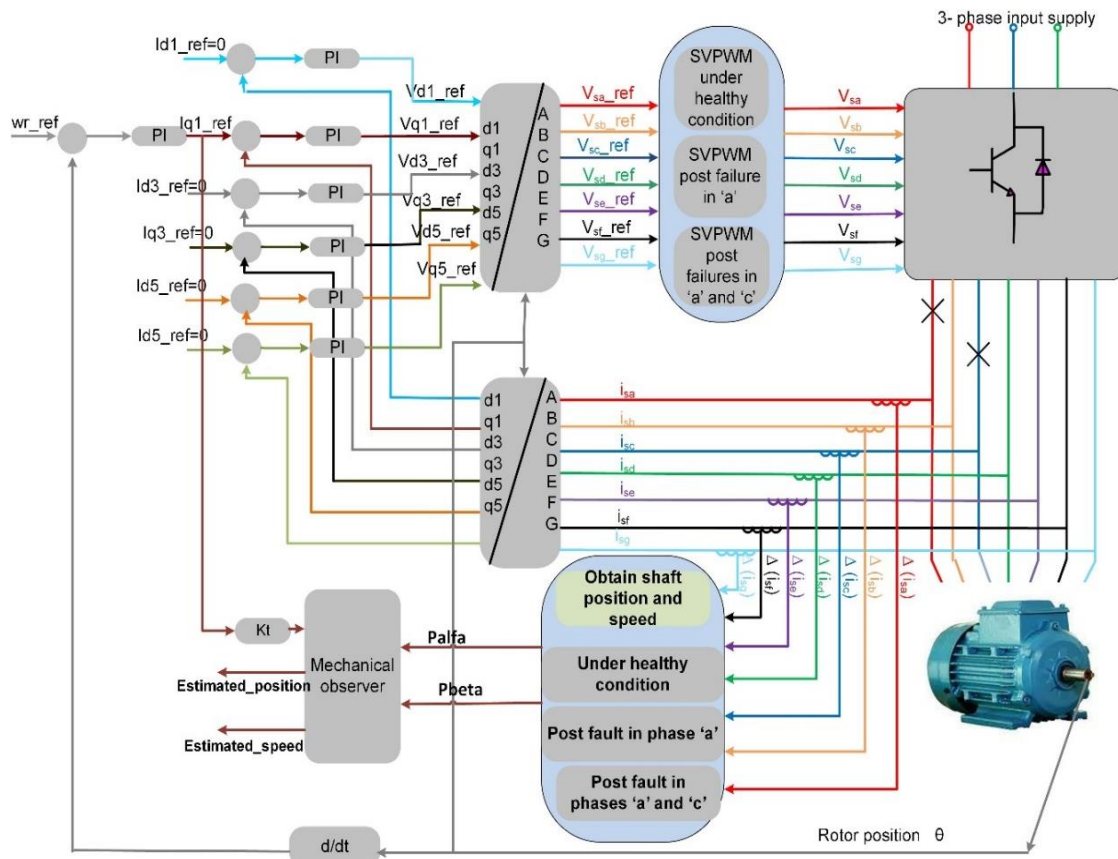

Figure 13. The control structure of the 7-phase drive to get the speed and position of the shaft after the loss of phases 'a' and 'c'

The 7-phase drive system depicted in Figure 13 was simulated and the results are illustrated in Figure 14. The 7-phase motor was rotating at 120 rpm speed and under healthy operating conditions. In this case, the 7-phase control technique presented in [36] to control the inverter and to estimate the shaft position and speed were utilized. At $t = 2\ s$, phase 'a' was lost and hence, the control technique presented in [41] was used to control the inverter and estimate the shaft speed and position. After that and while the motor continued to run after the fault in phase 'a', another fault was introduced in phase 'c' at $t = 3\ s$. In this case, the new SVPWM proposed in this article was utilized while the algorithm presented in [41] was used to estimate the shaft speed and position. The results show that the shaft position and speed were distorted and cannot be used to control the 7-phase motor. Finally, at $t = 3.5\ s$, the algorithm presented in the previous section was utilized to estimate the position and speed in the 7-phase drive after the loss in phases 'a' and 'c'. The results prove that the new algorithm succeeded to estimate the speed and position in the 7-phase drive after the failures in phases 'a' and 'c'. Also, the estimated position signals were cleaned and of the same quality as those obtained before that fault.
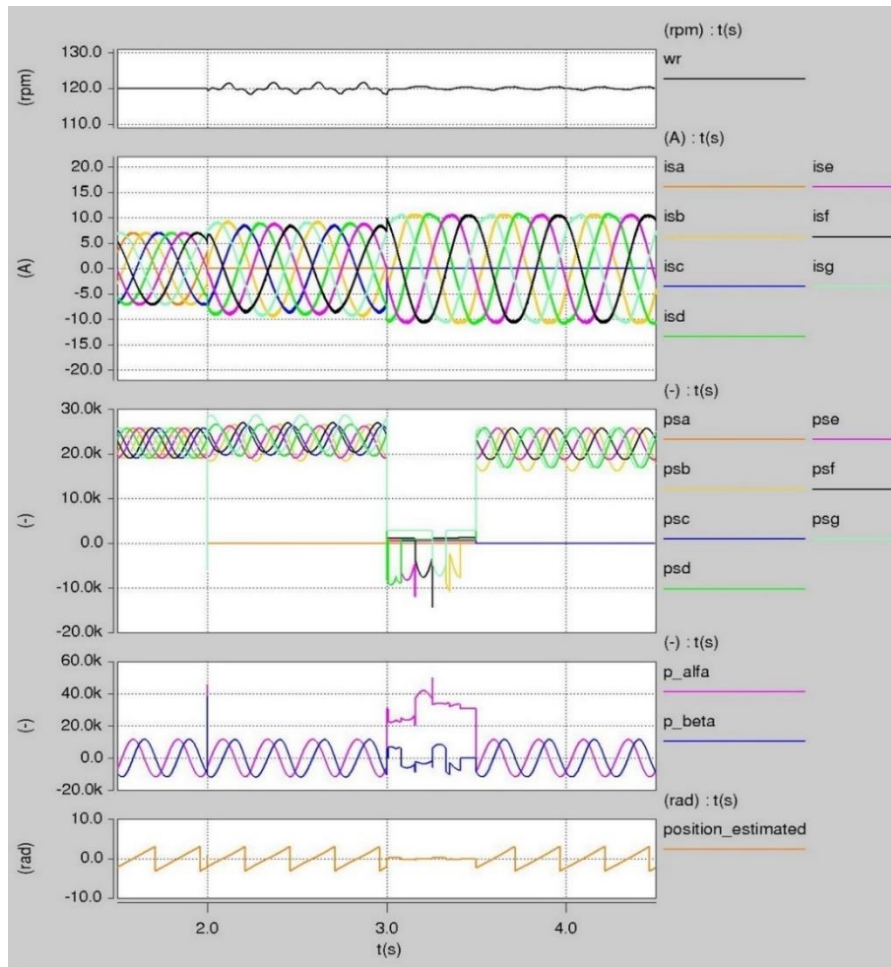
Figure 14. Obtaining shaft speed and position of the 7-phase drive post the failure in phases 'a' and 'c'

3.   RESULTS AND DISCUSSION
3.1.   Sensorless control of the 7-phase drive after the failures in phase 'a', phase 'c'

The sensorless control of the 7-phase drive in the cases of losing phases 'a' and 'c' was simulated using the SABER simulator according to the control schematic illustrated in Figure 15. When the motor was operated without failures, the 7-phase drive was controlled according to the technique presented in [36]. When a fault occurred in phase 'a', the 7-phase drive was controlled according to the technique presented in [41]. Finally, if phases 'a' and 'c' were lost due to a fault, the 7-phase drive will be controlled according to the FTC technique and the position and speed estimation algorithm that are presented in this article. The flow chart for implementing the whole system is shown in Figure 16.

Figure 17 shows the operation of the 7-phase drive at low speed after the failure in phases 'a' and 'c' in addition to the failure of the encoder. Initially, the 7-phase motor was running at 30 rpm under healthy operating conditions. The stator currents are identical to those given in (3). At $t = 2\ s$. An open circuit fault was introduced in phases 'a' and 'c' and at the same time, the new SVPWM was used as part of the FTC technique. The current waveforms were identical to those given in (5) and the controller was able to maintain the shaft speed at 30 rpm. Then a failure was introduced to the encoder at $t = 3\ s$ and therefore the algorithm presented in section 4 was used to obtain the shaft speed and position to be used in vector control of the 7-phase drive, as shown in Figure 15. The results show that the controller was able to keep the 7-phase drive running at the same speed after these faults. Finally, at $t = 4.5\ s$ and $t = 6\ s$, the wr_ref was set to 0 and -30 rpm respectively in the 7-phase drive while it was running under failures in phases 'a' and 'c' in addition to the failure of the encoder. The results obtained from the encoder prove that the 7-phase motor responded to these speed steps with good dynamic and stable behavior. Furthermore, the result proves that the robustness of the drive has been significantly increased by using the FTC technique and the algorithm to get the position that is presented in this paper.
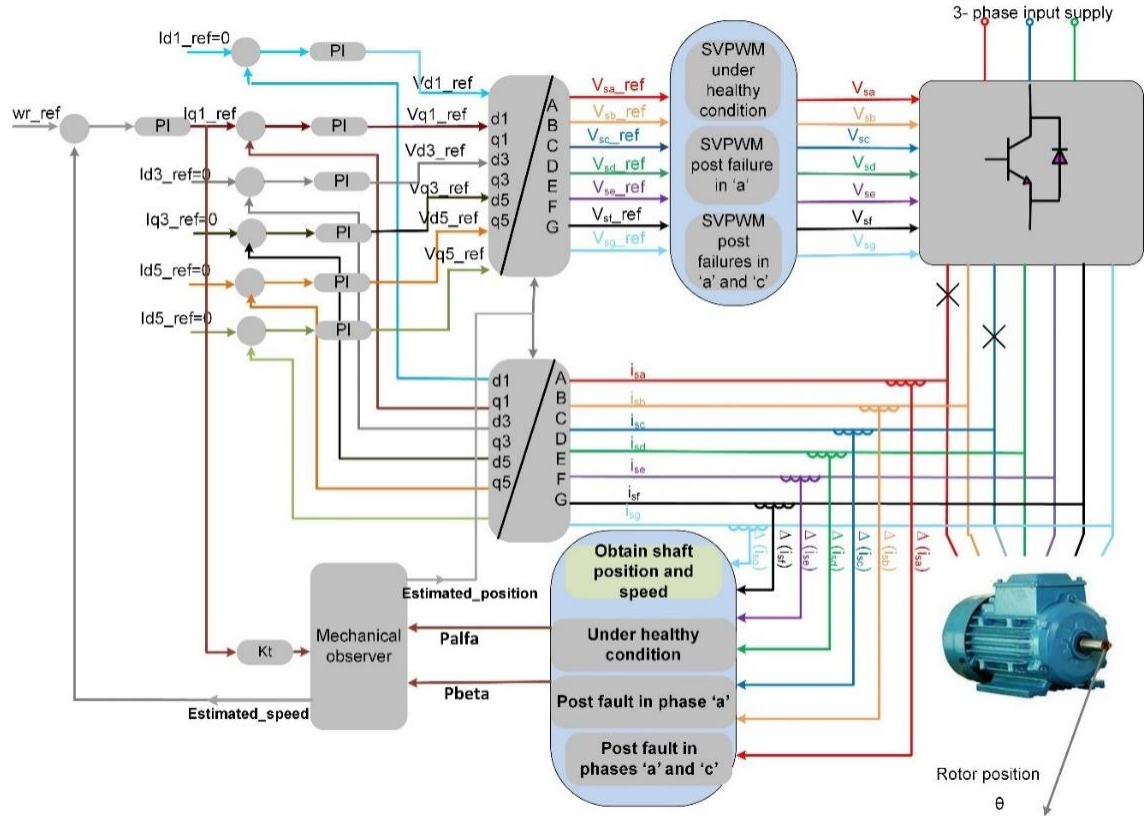
Figure 15. Control schematic to obtain sensorless operation of the 7-phase drive after the loss of phases 'a' and 'c'
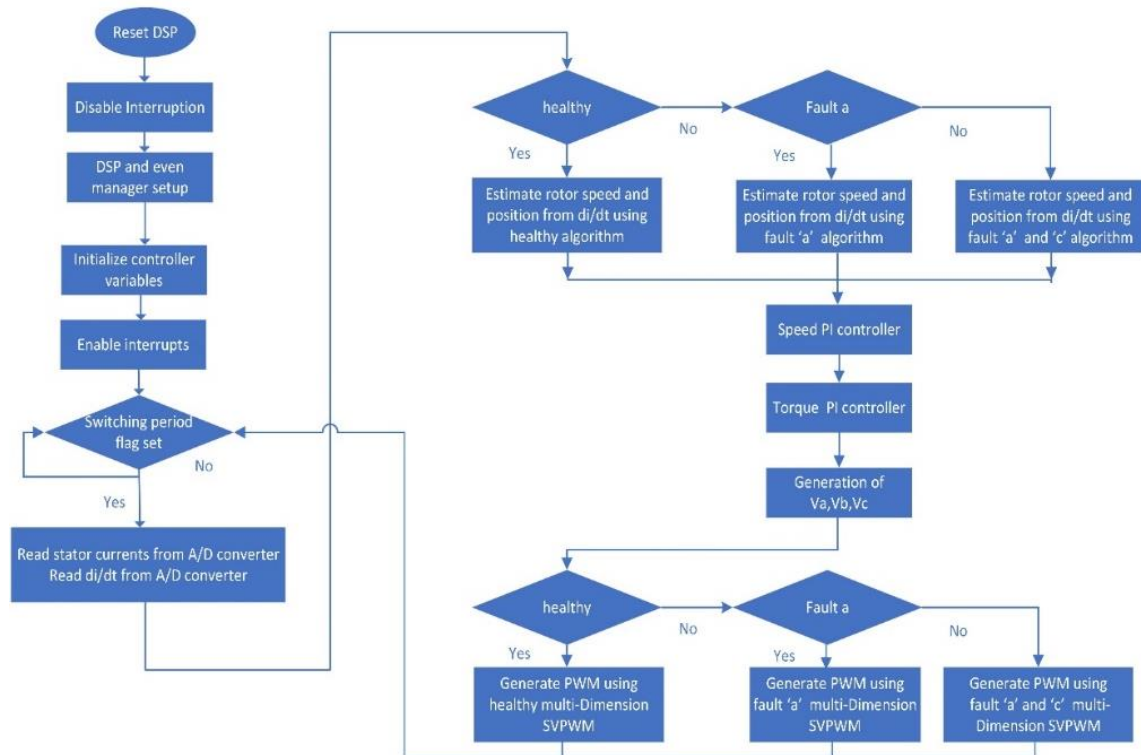

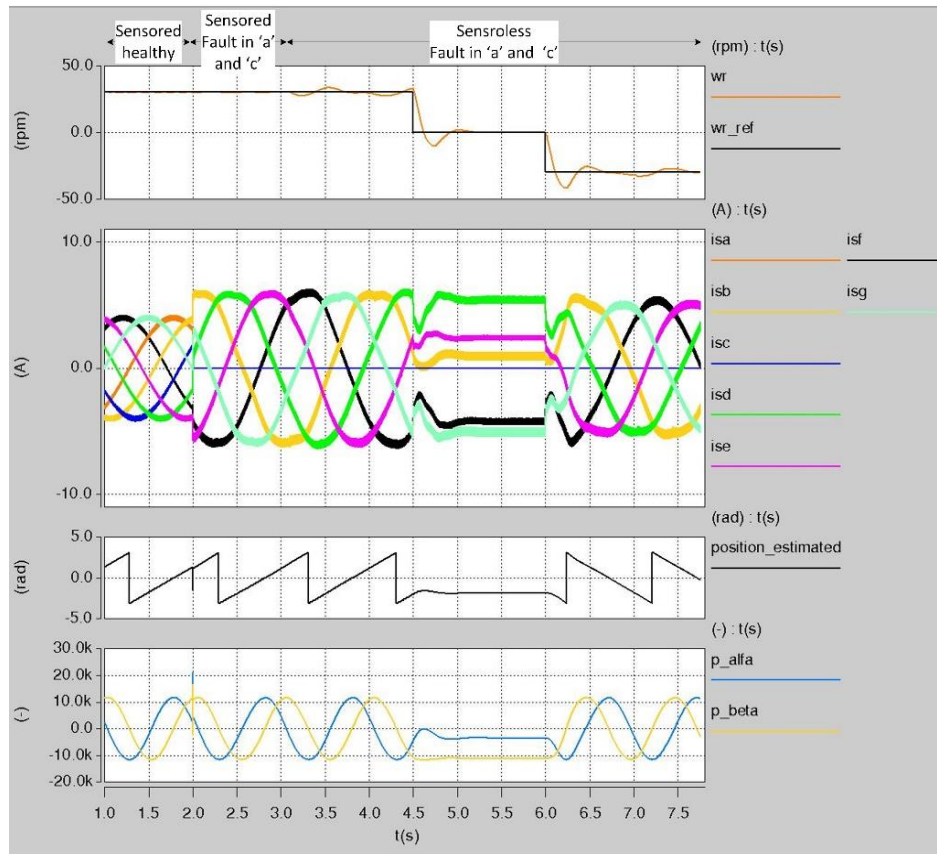Figure 16. Flow chart for the hardware implementation of the 7-phase drive post of three failures

Figure 17. Sensorless low-speed control of 7-phase drives under fault in phases 'a' and 'c'

Figure 18 shows the results of the 7-phase inverter subjected to different types of faults while running at a higher speed than depicted in Figure 17. The motor was operating at speed of 250 rpm and half the rated load without faults. At $t = 1\,s$, an-open circuit faults were introduced into phases 'a' and 'c'. The motor maintains operation at the same speed with minimum speed ripple. The current is also controlled to be identical to the values given in (5) by using the FTC technique proposed in this paper (i.e., by the new SVPWM). At $t = 1.5\,s$, wr_ref was set to 0. The measured speed (wr) shows that the 7-phase drive responds to these speed steps with good dynamic and steady-state behavior. Then, at $t = 3\,s$, while the motor was at standstill and phases 'a' and 'c' were lost due to a fault, another fault occurred in the 7-phase drive, namely the fault in the encoder. In this case, the algorithm presented in the previous section was utilized to determine the shaft speed and position in case of encoder fault to be used in the vector control. The results show that the speed of the 7-phase drive was maintained at zero. Finally, at $t = 3.5\,s$, while the 7-phase motor was running after the faults in phases 'a' and 'c' and the fault in the encoder, w_ref was changed from 0 to 250 rpm. The transient and steady-state performance of the 7-phase drive system proves that the behavior after the faults is at the same quality as the performance of the drive system when it is running without faults.

The results depicted in Figure 19 prove the ability of the 7-phase drive to maintain the speed when a load step was suddenly applied to the 7-phase drive system while it was running post the failures in phases 'a' and 'c' in addition to the failure of the encoder. Firstly, the motor was rotating at 100 rpm without faults. At $t = 1.5\,s$, faults occurred in phases 'a' and 'c' in the 7-phase drive at the same time the FTC technique that is proposed in this paper (new SVPWM) was utilized. Then, at $t = 2\,s$, while the two phases 'a' and 'c' of the 7-phase drive were faulted, a load disturbance was applied to it and removed after 0.5 s. after that, at $t = 3.5\,s$, the additional fault occurred in the 7-phase drives which is the encoder fault. In this case, the speed and position of the 7-phase drive were estimated using the technique presented in the previous section and used instead of those obtained using the encoder. Finally, at $t = 4\,s$, while the 7-phase drive was running post the above-mentioned faults, a load step was implemented and removed at $t = 4.5\,s$. The measured speed of the 7-phase drive obtained from the encoder illustrated in Figure 19 proves that during the whole test the 7-phase drive system could maintain the speed even under the extreme condition such as running under faults in phases 'a' and 'c' in addition to the fault in the encoder and at the same time applying the load disturbance.
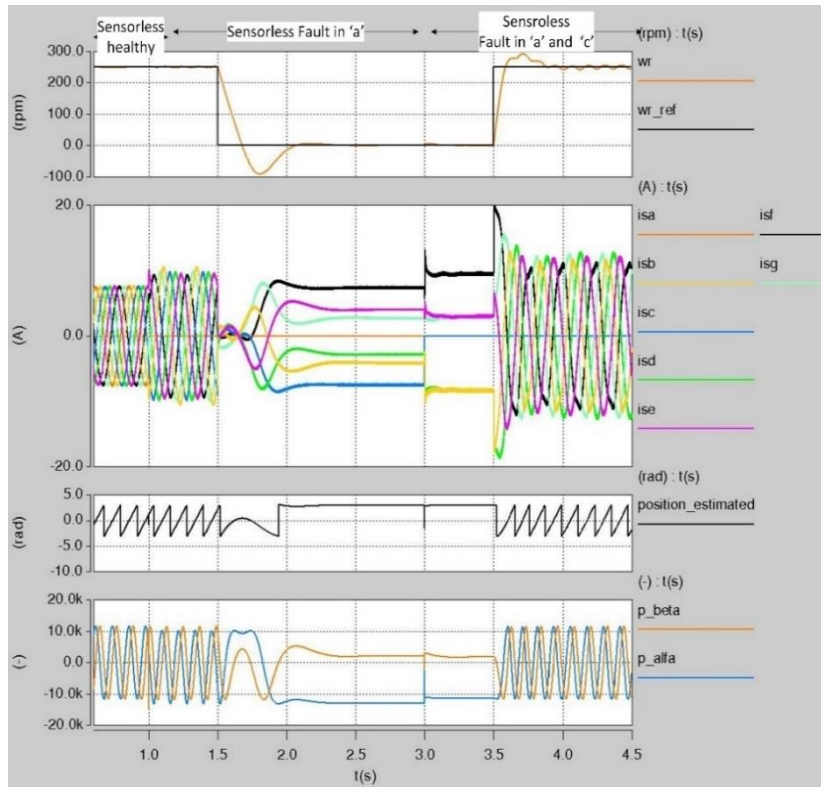
Figure 18. Sensorless operation of the 7-phase drive post the failures in phases 'a' and 'c' and during the demanding of high-speed steps
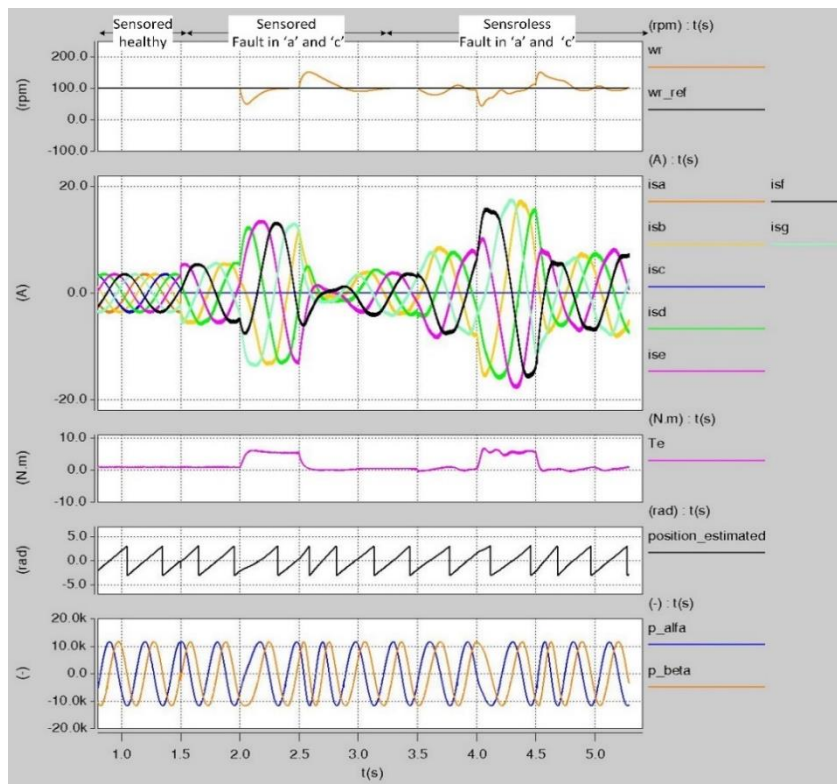

Figure 19. Sensorless operation of the 7-phase drives when the phases 'a' and 'c' are faulted during steps in the load toque

4.   CONCLUSION

This article has outlined a new FTC technique for the 7-phase PMS drive to significantly enhance its robustness by maintaining its performance post the faults in phases 'a' and 'c' in addition to the fault in the encoder. This is achieved by implementing two FTC techniques. The first one is represented in developing a new SVPWM technique in the cases of faults in phases 'a' and 'c' to obtain a new distribution of currents to minimize the inverter current. The second one is represented in developing a new algorithm to estimate the speed and position in the 7-phase drive in the cases of a failure in the encoder while phases 'a' and 'c' are faulted. The results have shown that the ripple in speed post the faults in phases 'a' and 'c' only was ±4 rpm and this ripple will reach ±10 rpm if the fault is introduced to the encoder too. Moreover, the results have shown that the performance of the 7-phase drive with and without faults was almost at the same quality. Finally, it should *h* mentioned that these techniques can be implemented quite easily (i.e., software modifications) and can be applied to the induction motor (IM) too.

REFERENCES

[1]   M. Villani, M. Tursini, G. Fabri, and L. Castellini, "Multi-phase fault tolerant drives for aircraft applications," in *Electrical Systems for Aircraft, Railway and Ship Propulsion*, Oct. 2010, pp. 1–6, doi: 10.1109/ESARS.2010.5665246.
[2]   P. W. Wheeler, "Multiphase induction motor drives," in *IET Chennai 3rd International Conference on Sustainable Energy and Intelligent Systems (SEISCON 2012)*, 2012, vol. 15, no. 6, doi: 10.1049/cp.2012.2256.
[3]   I. Subotic, N. Bodo, E. Levi, and M. Jones, "Onboard integrated battery charger for EVs using an asymmetrical nine-phase machine," *IEEE Transactions on Industrial Electronics*, vol. 62, no. 5, pp. 3285–3295, May 2015, doi: 10.1109/TIE.2014.2345341.
[4]   G. Zhang, W. Hua, M. Cheng, and J. Liao, "Design and comparison of two six-phase hybrid-excited flux-switching machines for EV/HEV applications," *IEEE Transactions on Industrial Electronics*, vol. 63, no. 1, pp. 481–493, Jan. 2016, doi: 10.1109/TIE.2015.2447501.
[5]   A. S. Abdel-Khalik, M. A. Elgenedy, S. Ahmed, and A. M. Massoud, "An improved fault-tolerant five-phase induction machine using a combined star/pentagon single layer stator winding connection," *IEEE Transactions on Industrial Electronics*, vol. 63, no. 1, pp. 618–628, Jan. 2016, doi: 10.1109/TIE.2015.2426672.
[6]   A. Cavagnino, Z. Li, A. Tenconi, and S. Vaschetto, "Integrated generator for more electric engine: design and testing of a scaled-size prototype," *IEEE Transactions on Industry Applications*, vol. 49, no. 5, pp. 2034–2043, Sep. 2013, doi: 10.1109/TIA.2013.2259785.
[7]   X. Xue, W. Zhao, J. Zhu, G. Liu, X. Zhu, and M. Cheng, "Design of five-phase modular flux-switching permanent-magnet machines for high reliability applications," *IEEE Transactions on Magnetics*, vol. 49, no. 7, pp. 3941–3944, Jul. 2013, doi: 10.1109/TMAG.2013.2244201.
[8]   X. Huang, A. Goodman, C. Gerada, Y. Fang, and Q. Lu, "Design of a five-phase brushless DC motor for a safety critical aerospace application," *IEEE Transactions on Industrial Electronics*, vol. 59, no. 9, pp. 3532–3541, Sep. 2012, doi: 10.1109/TIE.2011.2172170.
[9]   L. Shao, W. Hua, N. Dai, M. Tong, and M. Cheng, "Mathematical modeling of a 12-phase flux-switching permanent-magnet machine for wind power generation," *IEEE Transactions on Industrial Electronics*, vol. 63, no. 1, pp. 504–516, Jan. 2016, doi: 10.1109/TIE.2015.2461514.
[10]   A. Pantea *et al.*, "Six-phase induction machine model for electrical fault simulation using the circuit-oriented method," *IEEE Transactions on Industrial Electronics*, vol. 63, no. 1, pp. 494–503, Jan. 2016, doi: 10.1109/TIE.2015.2493727.
[11]   H. S. Che, M. J. Duran, E. Levi, M. Jones, W. P. Hew, and N. A. Rahim, "Postfault operation of an asymmetrical six-phase induction machine with single and two isolated neutral points," *IEEE Transactions on Power Electronics*, vol. 29, no. 10, pp. 5406–5416, Oct. 2014, doi: 10.1109/TPEL.2013.2293195.
[12]   H. S. Che, E. Levi, M. Jones, W. P. Hew, and N. A. Rahim, "Current control methods for an asymmetrical six-phase induction motor drive," *IEEE Transactions on Power Electronics*, vol. 29, no. 1, pp. 407–417, Jan. 2014, doi: 10.1109/TPEL.2013.2248170.
[13]   I. Gonzalez-Prieto, M. J. Duran, H. S. Che, E. Levi, M. Bermudez, and F. Barrero, "Fault-tolerant operation of six-phase energy conversion systems with parallel machine-side converters," *IEEE Transactions on Power Electronics*, vol. 31, no. 4, pp. 3068–3079, Apr. 2016, doi: 10.1109/TPEL.2015.2455595.
[14]   A. Tani, M. Mengoni, L. Zarri, G. Serra, and D. Casadei, "Control of multiphase induction motors with an odd number of phases under open-circuit phase faults," *IEEE Transactions on Power Electronics*, vol. 27, no. 2, pp. 565–577, Feb. 2012, doi: 10.1109/TPEL.2011.2140334.
[15]   F. Baudart, B. Dehez, E. Matagne, D. Telteu-Nedelcu, P. Alexandre, and F. Labrique, "Torque control strategy of polyphase permanent-magnet synchronous machines with minimal controller reconfiguration under open-circuit fault of one phase," *IEEE Transactions on Industrial Electronics*, vol. 59, no. 6, pp. 2632–2644, Jun. 2012, doi: 10.1109/TIE.2011.2170393.
[16]   H. Jia, J. Yang, R. Deng, and Y. Wang, "Loss investigation for multiphase induction machine under open-circuit fault using field–circuit coupling finite element method," *Energies*, vol. 14, no. 18, Sep. 2021, doi: 10.3390/en14185686.
[17]   J.-R. Fu and T. A. Lipo, "Disturbance free operation of a multiphase current regulated motor drive with an opened phase," in *Conference Record of the 1993 IEEE Industry Applications Conference Twenty-Eighth IAS Annual Meeting*, 1993, vol. 1, pp. 637–644, doi: 10.1109/IAS.1993.298884.
[18]   L. Zheng, J. E. Fletcher, and B. W. Williams, "Current optimization for a multi-phase machine under an open circuit phase fault condition," in *3rd IET International Conference on Power Electronics, Machines and Drives (PEMD 2006)*, 2006, vol. 2006, pp. 414–419, doi: 10.1049/cp:20060142.
[19]   A. Mohammadpour, S. Sadeghi, and L. Parsa, "A generalized fault-tolerant control strategy for five-phase PM motor drives considering star, pentagon, and pentacle connections of stator windings," *IEEE Transactions on Industrial Electronics*, vol. 61, no. 1, pp. 63–75, Jan. 2014, doi: 10.1109/TIE.2013.2247011.

[20] A. S. Abdel-Khalik, S. Ahmed, A. A. Elserougi, and A. M. Massoud, "Effect of stator winding connection of five-phase induction machines on torque ripples under open line condition," *IEEE/ASME Transactions on Mechatronics*, vol. 20, no. 2, pp. 580–593, Apr. 2015, doi: 10.1109/TMECH.2014.2303254.

[21] E. Ben Sedrine, J. Ojeda, M. Gabsi, and I. Slama-Belkhodja, "Fault-tolerant control using the GA optimization considering the reluctance torque of a five-phase flux switching machine," *IEEE Transactions on Energy Conversion*, vol. 30, no. 3, pp. 927–938, Sep. 2015, doi: 10.1109/TEC.2015.2402234.

[22] B. Tian, J. Hu, X. Huang, B. Zhou, and Q. An, "Performance comparison of three types of PWM techniques for a five-phase PMSM with a single-phase open circuited," in *2021 13th International Symposium on Linear Drives for Industry Applications (LDIA)*, Jul. 2021, pp. 1–5, doi: 10.1109/LDIA49489.2021.9505984.

[23] Q. Chen, G. Liu, W. Zhao, L. Qu, and G. Xu, "Asymmetrical SVPWM fault-tolerant control of five-phase PM brushless motors," *IEEE Transactions on Energy Conversion*, vol. 32, no. 1, pp. 12–22, Mar. 2017, doi: 10.1109/TEC.2016.2611620.

[24] H. Guzman *et al.*, "Comparative study of predictive and resonant controllers in fault-tolerant five-phase induction motor drives," vol. 63, no. 1, pp. 606–617, Jan. 2016, doi: 10.1109/tie.2015.2418732.

[25] L. Cheng, Y. Sui, P. Zheng, P. Wang, and F. Wu, "Implementation of postfault decoupling vector control and mitigation of current ripple for five-phase fault-tolerant PM machine under single-phase open-circuit fault," *IEEE Transactions on Power Electronics*, vol. 33, no. 10, pp. 8623–8636, Oct. 2018, doi: 10.1109/TPEL.2017.2782011.

[26] H. Zhou, W. Zhao, G. Liu, R. Cheng, and Y. Xie, "Remedial field-oriented control of five-phase fault-tolerant permanent-magnet motor by using reduced-order transformation matrices," *IEEE Transactions on Industrial Electronics*, vol. 64, no. 1, pp. 169–178, Jan. 2017, doi: 10.1109/TIE.2016.2599501.

[27] Q. Chen, W. Zhao, G. Liu, and Z. Lin, "Extension of virtual-signal-injection-based MTPA control for five-phase IPMSM into fault-tolerant operation," *IEEE Transactions on Industrial Electronics*, vol. 66, no. 2, pp. 944–955, Feb. 2019, doi: 10.1109/TIE.2018.2826473.

[28] Q. Chen, L. Gu, Z. Lin, and G. Liu, "Extension of space-vector-signal-injection-based MTPA control into SVPWM fault-tolerant operation for five-phase IPMSM," *IEEE Transactions on Industrial Electronics*, vol. 67, no. 9, pp. 7321–7333, Sep. 2020, doi: 10.1109/TIE.2019.2944066.

[29] M. Bermudez, I. Gonzalez-Prieto, F. Barrero, H. Guzman, X. Kestelyn, and M. J. Duran, "An experimental assessment of open-phase fault-tolerant virtual-vector-based direct torque control in five-phase induction motor drives," *IEEE Transactions on Power Electronics*, vol. 33, no. 3, pp. 2774–2784, Mar. 2018, doi: 10.1109/TPEL.2017.2711531.

[30] B. Tian, G. Mirzaeva, Q. T. An, L. Sun, and D. Semenov, "Fault-tolerant control of a five-phase permanent magnet synchronous motor for industry applications," *IEEE Transactions on Industry Applications*, vol. 54, no. 4, pp. 3943–3952, Jul. 2018, doi: 10.1109/TIA.2018.2820060.

[31] W. Huang, W. Hua, F. Chen, F. Yin, and J. Qi, "Model predictive current control of open-circuit fault-tolerant five-phase flux-switching permanent magnet motor drives," *IEEE Journal of Emerging and Selected Topics in Power Electronics*, vol. 6, no. 4, pp. 1840–1849, Dec. 2018, doi: 10.1109/JESTPE.2018.2845384.

[32] L. Zheng, J. E. Fletcher, B. W. Williams, and X. He, "A novel direct torque control scheme for a sensorless five-phase induction motor drive," *IEEE Transactions on Industrial Electronics*, vol. 58, no. 2, pp. 503–513, Feb. 2011, doi: 10.1109/TIE.2010.2047830.

[33] L. Zhang, Y. Fan, C. Li, A. Nied, and M. Cheng, "Fault-tolerant sensorless control of a five-phase FTFSCW-IPM motor based on a wide-speed strong-robustness sliding mode observer," *IEEE Transactions on Energy Conversion*, vol. 33, no. 1, pp. 87–95, Mar. 2018, doi: 10.1109/TEC.2017.2727074.

[34] A. H. Almarhoon, Z. Q. Zhu, and P. Xu, "Improved rotor position estimation accuracy by rotating carrier signal injection utilizing zero-sequence carrier voltage for dual three-phase PMSM," *IEEE Transactions on Industrial Electronics*, vol. 64, no. 6, pp. 4454–4462, Jun. 2017, doi: 10.1109/TIE.2016.2561261.

[35] G. Liu, C. Geng, and Q. Chen, "Sensorless control for five-phase IPMSM drives by injecting HF square-wave voltage signal into third harmonic space," *IEEE Access*, vol. 8, pp. 69712–69721, 2020, doi: 10.1109/ACCESS.2020.2986347.

[36] K. Saleh and M. Sumner, "Sensorless control of seven-phase PMSM drives using NSV-SVPWM with minimum current distortion," *Electronics*, vol. 11, no. 5, Mar. 2022, doi: 10.3390/electronics11050792.

[37] K. Saleh and M. Sumner, "Sensorless speed control of five-phase PMSM drives in case of a single-phase open-circuit fault," *Iranian Journal of Science and Technology, Transactions of Electrical Engineering*, vol. 43, no. 3, pp. 501–517, Sep. 2019, doi: 10.1007/s40998-018-00173-4.

[38] K. Saleh and M. Sumner, "Sensorless speed control of a fault-tolerant five-phase PMSM drives," *Electric Power Components and Systems*, vol. 48, no. 9–10, pp. 919–932, Jun. 2020, doi: 10.1080/15325008.2020.1825555.

[39] K.-Y. Chen, "Multiphase pulse-width modulation considering reference order for sinusoidal wave production," in *2015 IEEE 10th Conference on Industrial Electronics and Applications (ICIEA)*, Jun. 2015, pp. 1155–1160, doi: 10.1109/ICIEA.2015.7334281.

[40] W. N. W. A. Munim, H. S. Che, and W. P. Hew, "Fault tolerant capability of symmetrical multiphase machines under one open-circuit fault," in *4th IET Clean Energy and Technology Conference (CEAT 2016)*, 2016, vol. 2016, no. CP688, doi: 10.1049/cp.2016.1333.

[41] K. Saleh, "Seven-phase PMSM drives operation post twotypes of faults," *Applied Sciences*, vol. 12, no. 16, Aug. 2022, doi: 10.3390/app12167979.

[42] S. Xue, X. Wen, and Z. Feng, "A novel multi-dimensional SVPWM strategy of multiphase motor drives," in *2006 12th International Power Electronics and Motion Control Conference*, Aug. 2006, pp. 931–935, doi: 10.1109/EPEPEMC.2006.283280.

[43] P. Wang, P. Zheng, F. Wu, J. Zhang, and T. Li, "Research on dual-plane vector control of fivephase fault-tolerant permanent magnet machine," in *2014 IEEE Conference and Expo Transportation Electrification Asia-Pacific (ITEC Asia-Pacific)*, Aug. 2014, pp. 1–5, doi: 10.1109/ITEC-AP.2014.6941184.

[44] R. D. Lorenz and K. W. Van Patten, "High-resolution velocity estimation for all-digital, AC servo drives," *IEEE Transactions on Industry Applications*, vol. 27, no. 4, pp. 701–705, 1991, doi: 10.1109/28.85485.

BIOGRAPHIES OF AUTHORS

Kamel Saleh 🆔 🔳 SC ↻ was born in Tulkarm, Palestine, in 1980. He received the B.E. degree in electrical engineering from An-Najah National University in 2003. From 2003 to 2005, he worked as a planning engineer with the Palestinian Energy Authority. In 2005, He joined Nottingham University as a graduate student and obtained a master degree and Ph.D degree in electrical engineering in 2006 and 2009 respectively. From 2009 to 2010, he worked as a researcher with as a power electronics, control, and machine (PEMC) group at Nottingham university. Finally, in 2010 he joined the department of electrical engineering at An-Najah National university as a lecturer. Finally, in 2018 he was promoted to be associated professor. His current researches include sensorless control of multi-phase drive, multilevel inverters drive, DSTATCOM and renewable energy. He can be contacted at email: kamel.saleh@najah.edu.

Mark Sumner 🆔 🔳 SC ↻ received the B.Eng. degree in Electrical and Electronic Engineering from Leeds University in 1986 and then worked for Rolls Royce Ltd in Ansty, UK. Moving to the University of Nottingham. He completed his Ph.D in induction motor drives in 1990, and after working as a research assistant, was appointed Lecturer in October 1992. He is now Professor of Electrical Energy Systems. His research interests cover control of power electronic systems including sensorless motor drives, diagnostics and prognostics for drive systems, power electronics for enhanced power quality and novel power system fault location strategies. He can be contacted at email: mark.sumner@nottingham.ac.uk.